Bernd Rieger, Robert P.J. Nieuwenhuizen, and Sjoerd Stallinga

Image Processing and Analysis for Single-Molecule Localization Microscopy

Computation for nanoscale imaging

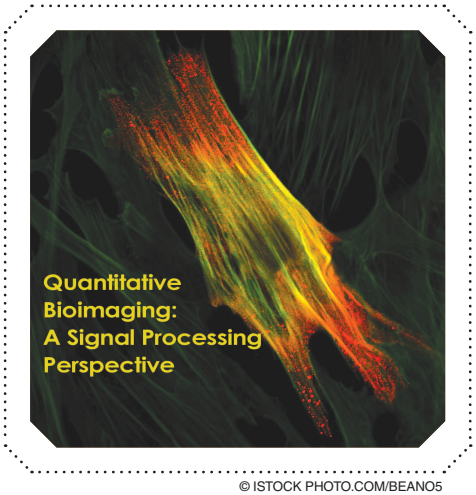

Fluorescence microscopy is currently the most important tool for visualizing biological structures at the subcellular scale. The combination of fluorescence, which enables a high imaging contrast, and the possibility to apply molecular labeling, which allows for a high imaging specificity, makes it a powerful imaging modality. The use of fluorescence microscopy has risen tremendously, in particular since the introduction of the green fluorescent protein (GFP) in the mid-1990s and the possibility to genetically engineer cells to express these proteins. Figure 1 shows the basic layout of a fluorescence microscope. Excitation light of a certain wavelength is reflected via a dichroic beamsplitter and projected onto the specimen via the objective lens of the microscope. The light is absorbed by the fluorescent labels and reemitted, slightly Stokes-shifted by ~10–100 nm, at a larger wavelength, typically a few nanoseconds later. The emission light is captured by the objective lens and directed toward the camera via the dichroic beamsplitter.

The resolution of a state-of-the-art microscope is limited by diffraction to a length scale $\lambda/2/\mathrm{NA}$, where λ is the emission wavelength, and $\mathrm{NA} = n \sin(\alpha)$ is the so-called numerical aperture (NA) of the microscope, where n is the refractive index of the immersion medium n and α is the marginal ray angle of the collected beam (see Figure 1). For visible light and high-NA immersion objectives, this gives resolutions ~200 nm. While this is sufficient for imaging many subcellular structures, it is insufficient for providing an image of the molecular machinery that underlies the functioning of the cell. Electron microscopy, however, can reveal image detail on the order of nanometers but does not allow live-cell imaging nor efficient specific labeling.

Over the last decade, a number of optical nanoscopy techniques have been proposed to bridge the resolution gap between electron and conventional light microscopy. Localization microscopy is one of these superresolution techniques [1]–[4]. These techniques rely on the localization of single fluorescent molecules, which was

Digital Object Identifier 10.1109/MSP.2014.2354094
Date of publication: 5 December 2014

already commonly done, e.g., in the field of single particle tracking before the advent of localization microscopy [5]. In localization microscopy, the fluorescent labels are photochemically manipulated to switch on and off stochastically, such that at each instant in time only a sparse subset of all molecules is in the on-state in which they can fluoresce. By now there is a whole plethora of stochastic switching mechanisms and suitable fluorescent labels [4]. The required ratio of on/off times to see only single emitters in a region of size λ/NA depends on the labeling density, camera frame time, etc., but is typically fewer than 1/100. Recording many frames of blinking emitting molecules thus provides a sequence of images of different random subsets of all molecules. The active molecules appear as well-separated spots that can be identified and processed to provide the position of the molecules. The localization precision is on the order of $\lambda/\mathrm{NA}/\sqrt{N_{\mathrm{ph}}} \approx 10$ nm with N_{ph} the number of detected photons (typically a few hundred to a few thousand). Assembling the localization data obtained from all frames into one visualization of the final superresolution image reveals details on the length scale of 10–100 nm; this is about one order below the diffraction limit of conventional light microscopy.

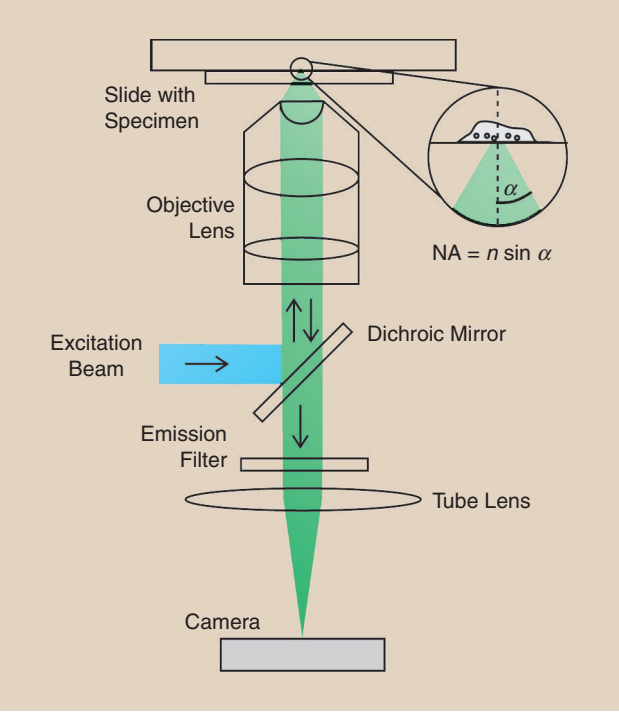

[FIG1] The schematics of an epi-fluorescence light microscope. The excitation light is focused onto the sample and the emission light is captured by the same lens and recorded on a camera. The dichroic mirror is chosen such that it reflects the excitation light but transmits the fluorescent emission light, which is of a slightly larger wavelength. The objective is characterized by the NA, which combines the refractive index of the immersion medium n and the maximum angle α at which light is captured.

THE NECESSARY TECHNOLOGY FOR LOCALIZATION MICROSCOPY IS NOT PROHIBITIVE: A STATE-OF-THE-ART SETUP ONLY REQUIRES A FLUORESCENCE MICROSCOPE, POWERFUL LIGHT SOURCES, AND A CAMERA WITH HIGH QUANTUM EFFICIENCY AND LOW READOUT NOISE.

The necessary technology for localization microscopy is not prohibitive: a state-of-the-art setup only requires a fluorescence microscope, powerful light sources, and a camera with high quantum efficiency and low readout noise. Next to this hardware, software for image processing and analysis is essential for extracting the desired molecular locations in a robust, optimal, and fast way. In this review article, we detail the image processing and workflow from raw camera frames to the visualization and quantitative analysis of the superresolution image. Figure 2 shows an overview of this workflow.

THE IMAGE PROCESSING PIPELINE

SEGMENTATION

The first step in processing the raw frames consists of identifying and segmenting regions of interest (ROIs) that contain the emissions of single fluorescent emitters. Usually this is done by thresholding the raw frames based on the pixel intensity relative to the (local) background noise level [1], [2]. Pixels in which the value is larger than a fixed threshold value or larger than a multiple of the background intensity b are taken as the center of ROIs that are used for localization of possible fluorophore positions in the next processing step.

Besides this basic thresholding approach, more advanced segmentation algorithms have also been proposed. In one proposed method, the raw images are first decomposed into wavelet maps to separate the fluorescence signal from bloblike sources from the background intensity and noise [6], [7]. Subsequently, ROIs are identified using a watershed segmentation algorithm.

Another approach to identifying ROIs makes explicit use of local hypothesis testing against the null hypothesis that a pixel belongs to the local background. This is achieved by computing the P-value for each pixel under the assumption that it is drawn from a normal distribution with the local mean and standard deviation of pixel values as parameters [8]. A related method that was proposed for single particle tracking employs a likelihood ratio test in each pixel. In this test, the ratio is computed between the likelihoods of the null hypothesis and that of the hypothesis of having a single emission from a fluorophore in the center of the pixel, assuming that the noise per pixel is Gaussian [9]. Under the null hypothesis, this ratio follows a chi-squared distribution. Pixels are thus thresholded based on the P-value of the chi-squared distribution for the likelihood ratio value of that pixel.

Segmentation algorithms typically assume a locally uniform background intensity. This is reasonable if the ROI is only a few pixels wide, unless there is a high degree of autofluorescence and the fluorophores themselves are relatively dim. For such cases, temporal median filtering has been proposed as a method for estimating the local background intensity [10].

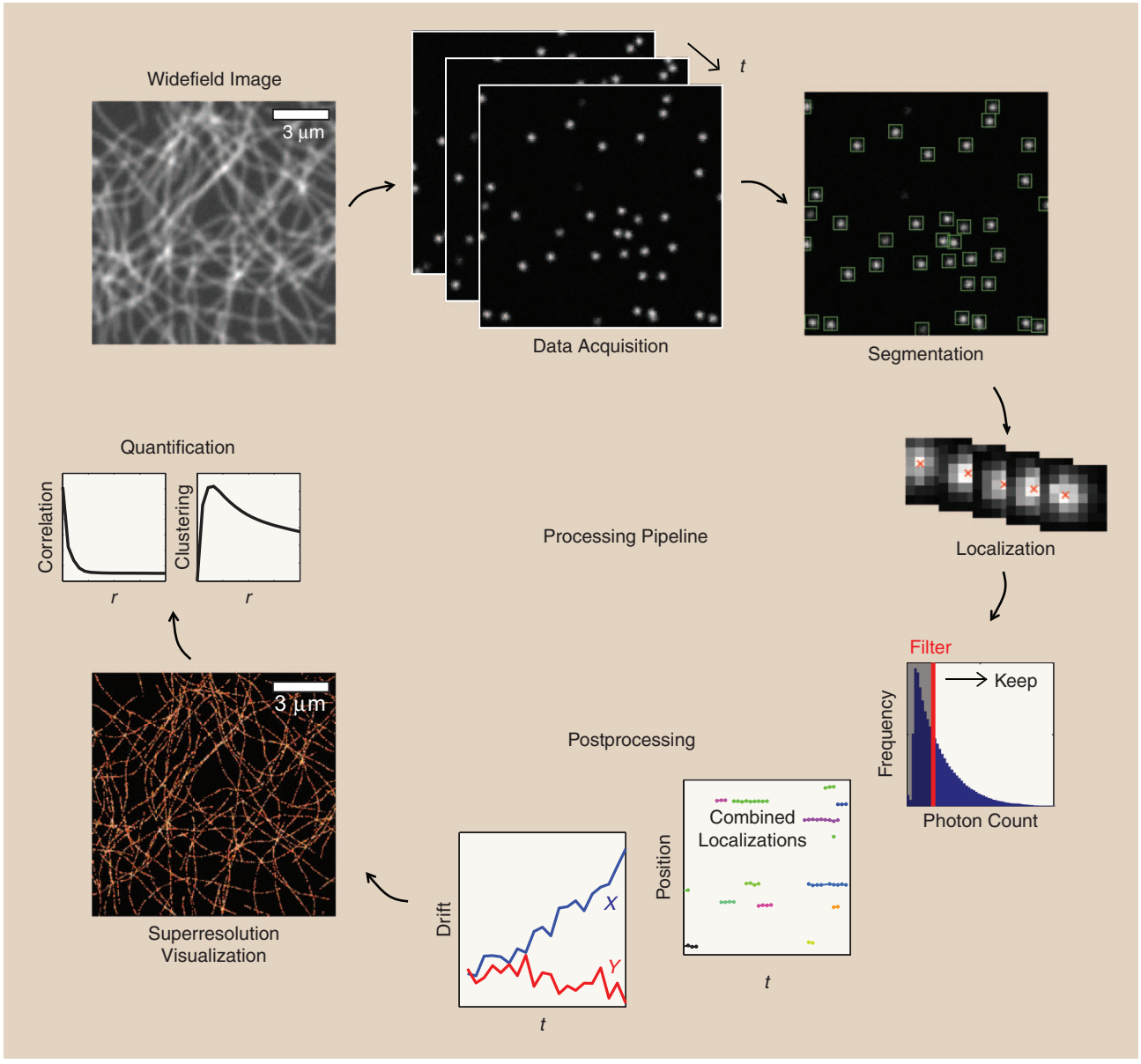

[FIG2] The complete pipeline for generating a 2-D superresolution image based on raw frames of sparsely activated fluorophores. The consecutive steps in this pipeline are acquisition of raw data, segmentation of ROIs, localization of potential fluorophores in the ROIs, postprocessing of the localizations (e.g., filtering, frame connection, drift correction), and visualization of the localizations.

SINGLE-MOLECULE LOCALIZATION

Once ROIs in the raw data have been segmented, the next step is to estimate the positions of the emitting fluorescent molecules in these regions. The most common approaches for this are the center of mass (CM) algorithm and algorithms that fit a point spread function (PSF) model to the data with a (weighted) least-squares (LS) estimator or a maximum likelihood estimator (MLE).

The CM algorithm computes the center of the intensity distribution. In the absence of any background intensity, this estimate corresponds well to the emitter's true location. However, for nonnegligible background intensities, this leads to a bias toward the CM of the background intensity, which is usually in the center of the ROI. Therefore the local background intensity needs to be estimated and subtracted before the CM can be computed.

LS and MLE algorithms attempt to fit a PSF model to the pixel intensities in a ROI. Typically the PSF model consists of a circularly symmetric Gaussian function for two-dimensional (2-D) localization microscopy

$$\mathrm{PSF}(x, y) = \frac{1}{2\pi\sigma_g^2} e^{-\frac{(x-x_c)^2+(y-y_c)^2}{2\sigma_g^2}}. \tag{1}$$

Here the parameters x_c and y_c denote the position of the emitter in the x- and y-direction and σ_g specifies the width of the PSF. The Gaussian PSF model is not derived from optical theory but is instead chosen for its conceptual simplicity and computational

efficiency. However, for typical imaging conditions, the Gaussian PSF approximates the theoretical PSF sufficiently well for accurate and precise localization [11], [12].

From the PSF model follows the expected intensity μ_k per pixel k that is fitted to the data

$$\mu_k = I_0 \int_{A_k} \mathrm{PSF}(u, v)\, du dv + b, \tag{2}$$

where I_0 denotes the sum intensity of the fluorophore, b the expected background photon count, and the integration runs over the area A_k of the kth pixel. The parameters that are to be estimated are thus x_c, y_c, I_0, b, and possibly σ_g.

In addition to an optical model for μ_k, fitting the PSF model to the data also requires a noise model for the imaging system. LS algorithms implicitly assume a Gaussian noise model, whereas the slower but more precise MLE algorithms assume a Poissonian noise model. The latter algorithms can be implemented on a graphical processing unit (GPU) to estimate the positions of many emitters in parallel and so achieve real-time computation [13].

An important issue in localization microscopy is the precision with which single fluorophores can be localized [14]–[16]. This is often analyzed using the concept of the Cramér–Rao lower bound (CRLB), which expresses the lowest variance of any unbiased estimator of a fluorophore's position for a given noise model [17]. For a Poissonian noise model, a good analytical approximation for this bound is given by [18]

$$\Delta x_{\mathrm{loc}}{}^2 = \frac{\sigma_e^2}{N}\left(1 + 4\tau + \sqrt{\frac{2\tau}{1+4\tau}}\right). \tag{3}$$

Here N is the number of signal photons, $\sigma_e^2 = \sigma_g^2 + a^2/12$ with a^2 is the pixel area, and τ is a normalized dimensionless background parameter $\tau = 2\pi\sigma_g^2 b/(Na^2)$ with b the number of background photons per pixel.

The noise in the commonly used scientific CMOS (sCMOS) and electron multiplying charge-coupled device (EMCCD) cameras deviates from the Poisson noise model in two important ways. sCMOS cameras suffer from a small amount of (pixel-dependent) Gaussian readout noise, which effectively acts as if b is increased with the variance of the readout noise [19]. EMCCD cameras suffer much less from readout noise due to the electron multiplication process. However, the stochasticity of this process also introduces so-called excess noise, which typically deteriorates the localization variance $\Delta x_{\mathrm{loc}}{}^2$ by a factor of two [20]. Balancing the effects of readout noise and excess noise implies that sCMOS cameras are preferred over EMCCD cameras, except in extremely low light conditions that are not typically encountered in localization microscopy [19]. Other considerations in choosing between cameras are that EMCCD cameras have a better photosensitivity, and that sCMOS cameras typically have a smaller physical pixel size and faster frame rate. Finally, sCMOS cameras require a calibration of the gain and readout noise of each pixel for accurate localization because they often vary substantially among different pixels on the same camera. For a more extensive introduction into the choice of localization algorithm, we refer to the review in [21].

POSTPROCESSING

After all the segmented ROIs have been processed by the localization algorithm, postprocessing of the raw localizations is needed. In the first postprocessing step, raw localizations are usually filtered. The goal of this filtering is to remove localizations that do not represent accurate position estimates of single fluorescent molecules, e.g., because they are due to overlapping emissions of multiple fluorophores or due to autofluorescence or residual sample contaminations. The filtering is usually done based on information that is returned by the localization algorithm, such as the estimated intensity of the fluorophore, the localization precision, the width of the PSF, as well as on the goodness of fit of the model to the data [1], [22]. The latter can be expressed as the (weighted) sum of squared errors between the fitted model and the data or as a ratio between the likelihoods of a fluorophore being present or absent.

In the second postprocessing step, localizations originating from the same fluorophore in consecutive frames of the raw image sequence are combined. This is attempted by searching for localizations in subsequent frames that are also spatially proximate, typically within a few times the estimated localization precision. The rationale for this operation is that fluorophores are often visible in multiple consecutive frames before transitioning into a stable dark state or photobleached state, whereas it is unlikely that a nearby fluorophore starts emitting during this time. In practice, fluorophores will not always be localized in all frames before going into a stable dark state, either due to failures of the localization algorithm or due to short blinking events during which the fluorophores briefly stop emitting light. Therefore, spatially proximate localizations are usually still combined if they are only a few frames apart in time [23].

A third common postprocessing operation is to correct for drift during the acquisition. Since localization microscopy experiments can last anywhere from a few minutes up to several hours, the sample often moves relative to the detector over distances larger than the localization precision of about 10 nm. This movement can be reduced with hardware solutions, e.g., by mechanically fixing the objective lens to the stage or by using a control system that actively controls the position of the sample in the image plane [24], [25]. Axial drift, causing the sample to drift out of focus, must be suppressed or controlled just as well as the lateral drift in the image plane.

One option is to add fiducial markers such as fluorescent microbeads to the sample that are visible during the entire acquisition [1]. These fiducial beads can then be localized and used to determine the position of the sample at each moment in time. Another option for drift correction is to estimate the shifts between images of the sample at different time points. This can be achieved by determining the maximum of the cross-correlation [24], [26], [27] between these images, which can either be raw camera images or superresolution images that visualize the localizations from these frames. The latter, however, is preferred for precision due to the larger high-frequency content of the superresolution image. The shift estimation should not be done between subsequent images only, as this leads to compounding of registration errors, but between image pairs further

apart in time. The main benefit of this approach is that it does not require any changes on the experimental side.

VISUALIZATION

The final step in the processing pipeline from raw data to superresolution image is the actual visualization of the data. For standard fluorescence microscopy acquisitions, this sampling occurs in the camera where the pixel positions along with the magnification determine the sampling of the image. In addition, the values per pixel are determined by the number of recorded photons per pixel bin that are translated into analog-to-digital units (ADUs) with a linear amplification factor. Unlike these standard fluorescence microscopy techniques, localization microscopy does not sample an image at pixel locations but produces a list of coordinates that represent the estimated fluorophore locations.

Several methods have been proposed for visualizing localizations in pixelated images that can be shown on a display device [28]. First, a scatterplot can be made of the localizations where the coordinates are plotted as a symbol in a Cartesian coordinate system [2]. Second, a histogram image can be made where the field of view is divided into square pixel bins and the number of localizations that fall in each bin is counted and used to assign intensity values to pixels. The resulting images often have a low signal-to-noise-ratio (SNR) per pixel and may cause aliasing problems if the resolution of the display device is too low. Therefore, these images are often blurred with a Gaussian kernel with a size on the order of the average estimated localization precision.

Third, localizations may be rendered as Gaussian blobs with a variable width proportional to their estimated localization precisions [1]. Alternatively, a fast method for obtaining a similar image is to sum several histogram images where the localizations are jittered for each image with a zero-mean normal probability distribution with a standard deviation proportional to the localization precision per localization [22]. These visualization methods have the benefit of conveying information about the precision of each localization in the images. However, additional factors such as uncorrected stage drift also lead to additional blurring. Therefore the blobs in these images cannot always be taken to represent the likelihood functions for the positions of the localized fluorophores.

Figure 3 shows an example where these visualization methods have been applied. In general, Gaussian rendering is the preferred method of visualization: it is best at conveying the information present in the data and it does not suffer much from aliasing with low-resolution displays.

ONE IMPORTANT EXTENSION OF 2-D LOCALIZATION MICROSCOPY IMAGING IS THE LOCALIZATION OF FLUOROPHORES IN THREE DIMENSIONS. THIS REQUIRES INFORMATION ABOUT THE AXIAL POSITION OF THE FLUOROPHORE IS PRESENT AND CAN BE EXTRACTED FROM THE RECORDINGS.

EXTENSIONS

Until now, the discussion focused in detail on the complete pipeline for generating a 2-D superresolution image based on raw frames of sparsely activated fluorophores. Here we will address several extensions of this pipeline involving localization in three dimensions, multicolor localization, and imaging with overlapping spots.

THREE-DIMENSIONAL LOCALIZATION

One important extension of 2-D localization microscopy imaging is the localization of fluorophores in three dimensions. This requires information about the axial position of the fluorophore is present and can be extracted from the recordings.

A first approach to this problem is to modify the optical setup such that the shape and/or size of the PSF can be uniquely related to the axial position of the fluorophore. The most common method to achieve this is to introduce astigmatism into the optical system [24]. This causes the minimum width of the PSF in the x- and y-direction to occur at different axial positions. The position can then be determined based on the ellipticity of the PSF.

A second approach to obtain the axial position is to modify the setup such that multiple images of the fluorophores with different

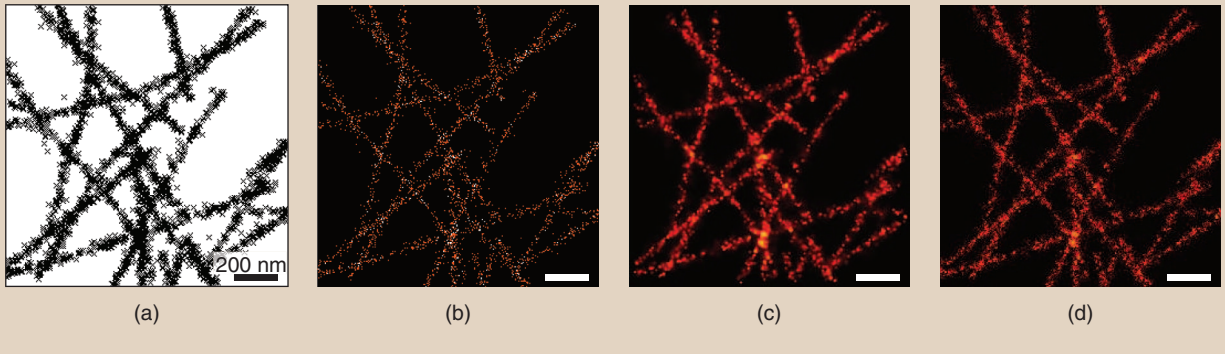

[FIG3] An illustration of commonly used visualization methods. (a) The scatterplot method, (b) histogram binning method, (c) Gaussian rendering method, and (d) jittered binning method. The scale bar is 200 nm.

defocus are simultaneously acquired. This is usually accomplished with a beam splitter that splits the emission light into two channels with different optical path lengths to the camera, such that the two images of the fluorophores are defocused with respect to each other [29].

For both these approaches to three-dimensional (3-D) localization, the PSF model that is used in the basic 2-D localization algorithm needs to be modified. The modified PSF model must provide a specification of the appearance of the fluorophore for the full range of axial positions under consideration and for all image channels on which it is observed. The PSF shapes for 3-D localization techniques may be difficult to describe in an analytic formula such as the Gaussian PSF model. An example of this is the double-helix PSF, where a spot doublet rotates with the axial focus position [30]. In such cases, the PSF can also be determined numerically or empirically. The latter approach then requires subsequent interpolation between the measured axial positions to provide a full specification of a fluorophore's appearance.

MULTICOLOR LOCALIZATION

Another important extension of the basic pipeline is the imaging of different labeled molecules in an experiment. A common method for doing this is to label these molecules with fluorophores with different emission spectra [31]. Wavelength dependent beam splitters are then inserted in the emission light path such that the light at different wavelengths ends up at different parts of the camera or at different cameras. The observed fluorophores can subsequently be classified into the different used species based on the fraction of the photons of each fluorophore ending up in the different color channels. Usually, though, the beam splitters are optimally selected such that each color channel only shows a single fluorescent species.

An important problem that arises when imaging fluorophores in different color channels is the registration of the various channels with respect to each other. This needs to be done with an accuracy comparable to the localization precision, which is typically 10% or less of the camera pixel size. A common solution employs fiducial markers that are visible in all color channels. These markers are first imaged and localized, and subsequently, a nonaffine mapping function is computed that maps the positions of the markers in one color channel to their positions in the other channels [32].

An alternative approach to multicolor imaging is to use photoswitchable dye pairs with different activator dyes but identical reporter dyes [31]. In this way, the wavelength of the illumination can be used to determine which dye pairs are activated and therefore which labeled molecules are imaged. The emitted light of all reporter dyes can then be imaged in a single image on the camera, thus circumventing chromatic aberration problems and obviating the need for a registration procedure between different images.

HIGH-DENSITY METHODS

A common problem when localizing fluorophores is that segmented ROIs contain overlapping spots of multiple active fluorophores. This issue is particularly important when the density of active fluorophores is high. Several solutions have been proposed that attempt to fit a PSF model to each of the spots in the ROI, either by fitting spots one by one [33] or by finding the model with the number of PSFs that best matches the data [34].

Several other methods for dealing with overlapping spots have been proposed that do not estimate fluorophore positions but rather estimate the density of fluorophores instead. One such approach is to deconvolve the entire raw data set [35]. This means that for each frame, a fluorophore density is estimated, which has the highest likelihood of producing the experimentally recorded data after convolution with the PSF. To achieve subdiffraction resolution, this density is sampled with a smaller pixel size than the experimental data. The estimation also incorporates a prior probability for the density per frame that promotes sparsity: because relatively few emitters are active in each frame, the solution should also have few pixels with nonzero density. A related approach to estimating the density is provided by compressive sensing [36], [37]. Unlike the deconvolution approach, an estimate $\rho(x, y)$ is made for each frame independently, which minimizes the balanced sum between a data misfit term and sparsity promoting "L1-norm" of the form $\sum_{x,y} |\rho(x, y)|$. A subtlety in these approaches is that, in principle, the final estimated density is a relative rather than an absolute estimation of the molecular density, as fluorophores can reappear in the on-state multiple times during the data acquisition.

The final approach to be mentioned here is called the *Bayesian analysis* of the blinking and bleaching (3B) method [38]. In this method, the on- and off-switching and bleaching behavior of each fluorophore is modeled as a Markov process. Using this model, many different estimates are made of the number of fluorophores, their positions, and their activity in each frame. These estimates are then all used to create a probability map of the positions of the fluorophores. A major drawback of this method is its high computational cost.

QUANTITATIVE IMAGE ANALYSIS

RESOLUTION QUANTIFICATION

Localization microscopy produces images that have a resolution below the diffraction limit. However, so far we have not answered this question: Exactly how far below the diffraction limit is the resolution in these images?

The apparent width of structures is clearly blurred on the scale of the localization precision. Additional blurring is introduced by sample drift and the nonzero size of the fluorescently labeled markers (e.g., antibodies). Another factor limiting resolution is that the molecules of interest are labeled with fluorophores at a finite density. In addition to this, usually not all of the target molecules are labeled and not all labels result in actual localizations. So, both the overall density of recorded labels and the different blurring factors influence what detail can be reliably discerned. It is noteworthy that the sampling theorem does not apply here: the localizations that are

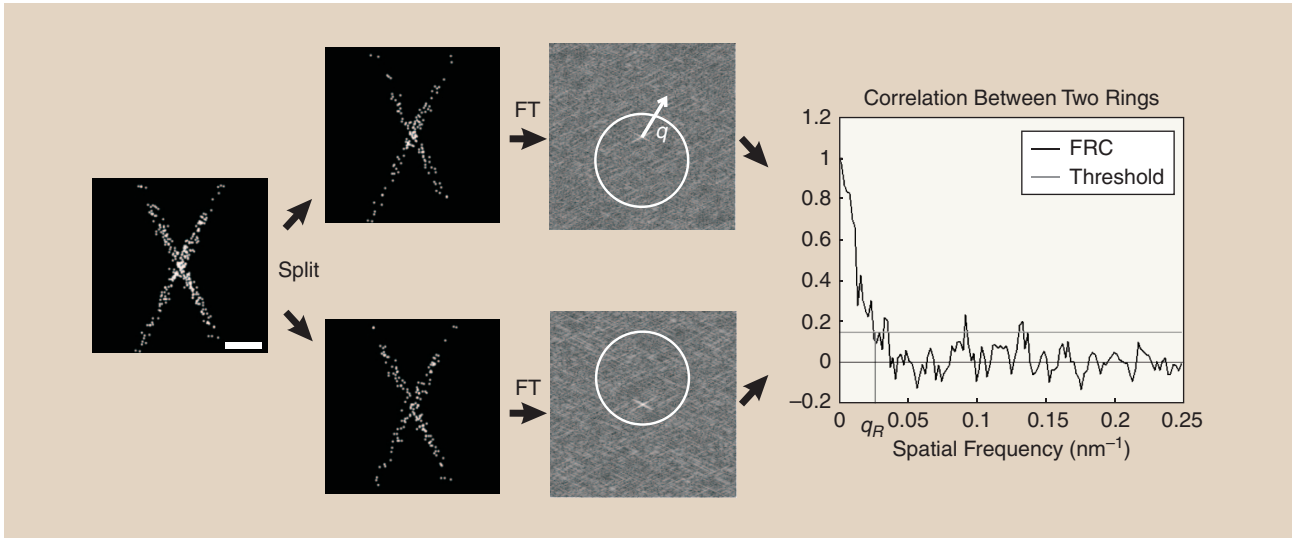

[FIG4] A schematic illustration of FRC resolution computation. The localizations are divided into two halves, and their Fourier transforms are correlated over the perimeters of circles in Fourier space of radius q. The resulting FRC curve decays with spatial frequency, and the image resolution is taken to be the inverse of the spatial frequency q_R where the FRC curve drops below the threshold 1/7.

obtained are positions rather than samples of a bandwidth limited density function.

Fourier ring correlation (FRC) provides a practical image-resolution measure that incorporates all of the aforementioned factors that influence the resolution [39]. To compute the FRC resolution, the full set of estimated fluorophore positions is divided into two independent subsets. An image is then made for each subset, yielding two subimages $f_1(x, y)$ and $f_2(x, y)$. Statistical correlation of their Fourier transforms $\hat{f}_1(\vec{q})$ and $\hat{f}_2(\vec{q})$ over the pixels on the perimeter of circles of constant spatial frequency magnitude $q = |\vec{q}|$ then gives the FRC

$$\mathrm{FRC}(q) = \frac{\sum\limits_{\vec{q}\in\text{circle}} \hat{f}_1(\vec{q})\hat{f}_2(\vec{q})^*}{\sqrt{\sum\limits_{\vec{q}\in\text{circle}} \hat{f}_1(\vec{q})^2}\sqrt{\sum\limits_{\vec{q}\in\text{circle}} \hat{f}_2(\vec{q})^2}}. \tag{4}$$

For low spatial frequencies, the FRC curve is close to unity, and for high spatial frequencies, noise dominates the data and the FRC decays to zero. The image resolution is defined as the inverse of the spatial frequency $R = 1/q_R$ for which the FRC curve drops below a given threshold. Various threshold criteria are in use in the field of cryo-EM, but the fixed threshold of $\mathrm{FRC}(q_R) = 1/7 \approx 0.143$ was empirically found to be the most appropriate for localization microscopy images. Thus the FRC resolution describes the length scale below which the image lacks signal content; smaller details are not resolved in the image. The steps needed to compute the FRC resolution are illustrated in Figure 4.

CLUSTER ANALYSIS

Another common quantification task for localization microscopy is cluster analysis. In this analysis, the objective is to assess the degree to which the imaged molecules cluster together. In other words, the question is: To what extent does the distance distribution between the molecules differ from that of randomly distributed molecules? The two most common analysis techniques used for this problem are the pair correlation function and techniques based on Ripley's K function. See Figure 5 for an illustrative example.

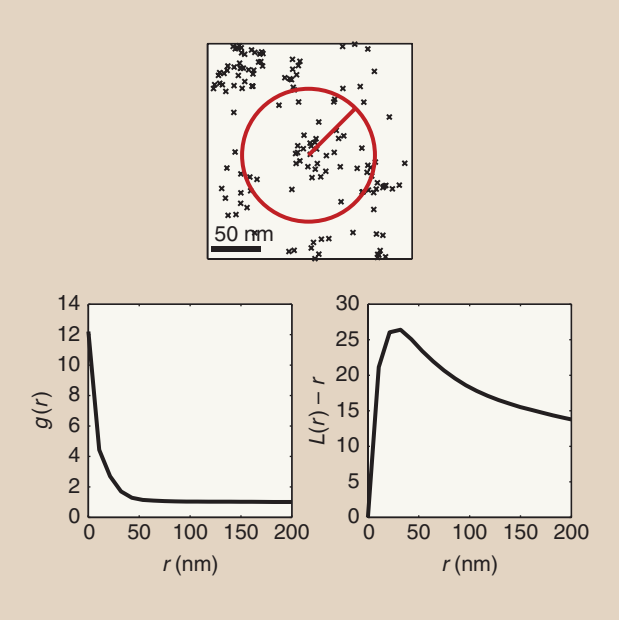

[FIG5] A schematic illustration of cluster analysis. The cross-correlation function $g(r)$ indicates the average density of localizations around each localization at a distance r. Ripley's K analysis considers the number of localizations within a distance r of each localization. The linearized version $L(r)$ is equal to r for randomly distributed localizations and thus allows for easy visualization of clustering of the localizations by plotting $L(r) - r$.

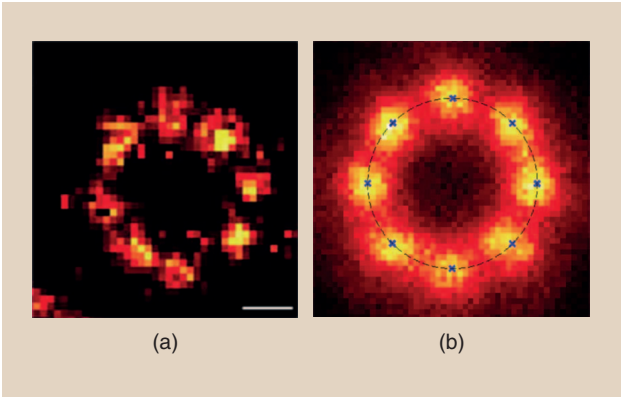

[FIG6] (a) A single superresolution image of a completely labeled nuclear pore complex (NPC) and (b) the sum of 426 of these superresolved and registered NPC images. The scale bar is 50 nm. (Image used with permission from [42].)

The pair-correlation function $g(r)$ describes the average number of localizations at a distance r from each other localization, normalized by the average density of localizations [40]

$$g(x, y) = \langle \rho(x', y')\rho(x' - x, y' - y)\rangle / \rho^2. \tag{5}$$

Here $\rho(x, y)$ is the density of localizations at position (x, y). When using the pair-correlation function to assess clustering, there are two important caveats that have to be taken into account. First, if fluorophores are localized multiple times then this will result in excess clustering on the length scale of the localization uncertainty which has to be accounted for. This will almost always be the case unless fluorescent proteins are used that are permanently photobleached after their first photoactivation. Second, the pair-correlation between localizations does not exactly reflect that of the actual labeled molecules due to the localization uncertainty.

A closely related alternative to pair-correlation analysis is provided by the use of Ripley's K function [41]. Ripley's K function measures the average number of localizations within a distance r from each other localization

$$K(r) = \frac{1}{N\rho}\sum_{i=1}^{N}\sum_{j\neq i}\delta_{i,j}, \tag{6}$$

where N is the number of localizations and $\delta_{i,j} = 1$ if the distance between localizations i and j is smaller than r and zero otherwise. Often, the linearized functions $L(r) = \sqrt{K(r)/\pi}$ or $H(r) = L(r) - r$ are used for data analysis, since the latter has an expected value of zero for a random distribution of localizations.

IDENTICAL STRUCTURE AVERAGING

The resolution of localization microscopy can even be further increased by image processing in case the field-of-view contains many copies of identical structures or macromolecules. All superresolution reconstructions from these structures can then be segmented and subsequently registered with respect to each other and added together. This results in one compound superresolution image of the structure with a very high effective localization density. This, in turn, increases the SNR and thus the resolution as detailed in the section "Resolution Quantification." In addition, this registration can deal with partially unoccupied labeling sites on the structure as long as the empty labeling sites are random and even these incomplete structures contribute to an increased SNR. An example of identical structure averaging is given by superresolution imaging of the NPC, which is the gateway between the cell nucleus and the cytoplasm; compare Figure 6(a) and (b) [42], [43]. The same idea of averaging biological identical structures, but with low SNR of each individual image, has been employed by Engelenburg et al. [44] to gain insight into the protein distribution within HIV.

OUTLOOK

As image processing and analysis is such an essential ingredient of superresolution microscopy, substantial efforts have already been dedicated to it over the years. The standard 2-D processing pipeline is now well established, but there are still significant opportunities for improvement. In particular, the detection of all suitable ROIs that contain single molecule events and the filtering of localization events are suitable topics, as these have been treated largely ad hoc rather than fundamentally. The reason that these tasks have been somewhat neglected is, in part, because a reasonably good superresolution reconstruction can be obtained without such a very fundamental treatment. The methods using deconvolution on the raw data instead circumvent this problem; however, they suffer from other drawbacks (see the section "High-Density Methods"). We see a need for fast and reliable identifications of ROIs especially for very weak signals (fewer than a few hundred photons) on substantial background. Such signals are typically encountered when imaging fluorescent proteins, while imaging at high frame rates for live cell observation or when imaging deeper inside a cell or tissue ($> 1\,\mu$m). We also foresee a rise for methods that deal with overlapping spots of proximate emitters, as higher active emitter densities are beneficial for faster and higher resolution imaging. Finally, quantitative image analysis methods in general and the use of prior knowledge in particular (as in the section "Identical Structure Averaging") may further open up the nanoscopic world for image-based exploration.

AUTHORS

Bernd Rieger (b.rieger@tudelft.nl) received the M.Sc. degree in physics from the Technische Universität München, Germany, in 1999. He received his Ph.D. degree in 2004 in image processing and analysis from Delft University of Technology, The Netherlands. After a postdoctoral position at the Max Planck Institute for Biophysical Chemistry, Göttingen, and a research position at FEI Electron Optics, Eindhoven, in 2006 he rejoined the Department of Imaging Physics at Delft University of Technology, where he is now an associate professor. His current research interests are the application of image analysis to optical nanoscopy and to electron microscopy.

Robert P.J. Nieuwenhuizen (r.p.j.nieuwenhuizen@tudelft.nl) received a B.Sc. degree in applied physics in 2008 (cum laude), an M.Sc. degree in applied physics in 2011 (cum laude), and an M.Sc. degree in management of technology in 2011 (cum laude), all

from Delft University of Technology, The Netherlands. He is currently a Ph.D. candidate in the Department of Imaging Physics at Delft University of Technology, under the supervision of Bernd Rieger and Sjoerd Stallinga, doing research on quantitation of localization microscopy.

Sjoerd Stallinga (s.stallinga@tudelft.nl) obtained his Ph.D. degree in 1995 from the University of Nijmegen after graduating from that university in 1993 on a theoretical study in liquid crystal physics. He worked from 1995 to 2008 as a senior scientist and project leader at Philips Research in Eindhoven on various optical topics, and, in 2009, he joined the Delft University of Technology, The Netherlands, as an associate professor in the Department of Imaging Physics. His current research interests are the analysis, design, and realization of computational optical imaging systems, with an emphasis on optical nanoscopy and digital pathology.

REFERENCES

[1] E. Betzig, G. Patterson, R. Sougrat, O. Lindwasser, S. Olenych, J. Bonifacino, M. Davidson, J. Lippincott-Schwartz, and H. Hess, "Imaging intracellular fluorescent proteins at nanometer resolution," *Science*, vol. 313, pp. 1643–1645, Sept. 2006.

[2] M. Rust, M. Bates, and X. Zhuang, "Sub-diffraction-limit imaging by stochastic optical reconstruction microscopy (STORM)," *Nat. Methods*, vol. 3, no. 10, pp. 793–795, 2006.

[3] S. T. Hess, T. P. K. Girirajan, and M. D. Mason, "Ultra-high resolution imaging by fluorescence photoactivation localization microscopy," *Biophys. J.*, vol. 91, no. 11, pp. 4258–4272, 2006.

[4] T. Klein, S. Proppert, and M. Sauer, "Eight years of single-molecule localization microscopy," *Histochem. Cell Biol.*, vol. 141, no. 6, pp. 561-575, 2014.

[5] M. J. Saxton and K. Jacobson, "Single-particle tracking: Applications to membrane dynamics," *Annu. Rev. Biophys. Biomolec. Struct.*, vol. 26, pp. 373–399, June 1997.

[6] J.-C. Olivo-Marin, "Extraction of spots in biological images using multiscale products," *Pattern Recogn.*, vol. 35, no. 9, pp. 1989–1996, 2002.

[7] I. Izeddin, J. Boulanger, V. Racine, C. Specht, A. Kechkar, D. Nair, A. Triller, D. Choquet, M. Dahan, and J. Sibarita, "Wavelet analysis for single molecule localization microscopy," *Opt. Express*, vol. 20, no. 3, pp. 2081–2095, 2012.

[8] Y. Li, Y. Ishitsuka, P. Hedde, and G. Nienhaus, "Fast and efficient molecule detection in localization-based super-resolution microscopy by parallel adaptive histogram equalization," *ACS Nano*, vol. 7, no. 6, pp. 5207–5214, 2013.

[9] A. Serge, N. Bertaux, H. Rigneault, and D. Marguet, "Dynamic multiple-target tracing to probe spatiotemporal cartography of cell membranes," *Nat. Methods*, vol. 5, no. 8, pp. 687–694, 2008.

[10] E. Hoogendoorn, K. Crosby, D. Leyton-Puig, R. Breedijk, K. Jalink, T. Gadella, and M. Postma, "The fidelity of stochastic single-molecule super-resolution reconstructions critically depends upon robust background estimation," *Sci. Rep.*, vol. 4, p. 3854, Jan. 2014.

[11] B. Zhang, J. Zerubia, and J.-C. Olivo-Marin, "Gaussian approximations of fluorescence microscope point-spread function models," *Appl. Opt.*, vol. 46, no. 10, pp. 1819–1829, 2007.

[12] S. Stallinga and B. Rieger, "Accuracy of the Gaussian point spread function model in 2D localization microscopy," *Opt. Express*, vol. 18, no. 24, pp. 24,461–24,476, 2010.

[13] C. Smith, N. Joseph, B. Rieger, and K. Lidke, "Fast, single-molecule localization that achieves theoretically minimum uncertainty," *Nat. Methods*, vol. 7, no. 5, pp. 373–375, 2010.

[14] R. E. Thompson, D. R. Larson, and W. W. Webb, "Precise nanometer localization analysis for individual fluorescent probes," *Biophys. J.*, vol. 82, no. 5, pp. 2775–2783, 2002.

[15] M. P. Gordon, T. Ha, and P. R. Selvin, "Single-molecule high-resolution imaging with photobleaching," *Proc. Natl. Acad. Sci. USA*, vol. 101, no. 17, pp. 6462–64654, 2004.

[16] H. Deschout, F. C. Zanacchi, M. Mlodzianoski, A. Diaspro, J. Bewersdorf, S. T. Hess, and K. Braeckmans, "Precisely and accurately localizing single emitters in fluorescence microscopy," *Nat. Methods*, vol. 11, no. 3, pp. 253–266, 2014.

[17] R. Ober, S. Ram, and S. Ward, "Localization accuracy in single-molecule microscopy," *Biophys. J.*, vol. 86, no. 2, pp. 1185–1200, 2004.

[18] B. Rieger and S. Stallinga, "The lateral and axial localization uncertainty in super-resolution light microscopy," *ChemPhysChem*, vol. 15, no. 4, pp. 664–670, 2014.

[19] F. Huang, T. Hartwich, F. Rivera-Molina, Y. Lin, C. Whitney, J. Long, P. Uchil, J. Myers, M. Baird, W. Mothes, M. Davidson, D. Toomre, and J. Bewersdorf, "Video-rate nanoscopy using sCMOS camera-specific single-molecule localization algorithms," *Nat. Methods*, vol. 10, no. 7, pp. 653–658, 2013.

[20] J. Chao, S. Ram, E. Ward, and R. Ober, "Ultrahigh accuracy imaging modality for super-localization microscopy," *Nat. Methods*, vol. 10, no. 4, pp. 335–338, 2013.

[21] A. Small and S. Stahlheber, "Fluorophore localization algorithms for super-resolution microscopy," *Nat. Methods*, vol. 11, no. 3, pp. 267–279, 2014.

[22] P. Krizek, I. Raska, and G. Hagen, "Minimizing detection errors in single molecule localization microscopy," *Opt. Express*, vol. 19, no. 4, pp. 3226–3235, 2011.

[23] P. Annibale, S. Vanni, M. Scarselli, U. Rothlisberger, and A. Radenovic, "Quantitative photo activated localization microscopy: Unraveling the effects of photoblinking," *PLoS ONE*, vol. 6, no. 7, p. e22678, 2011.

[24] B. Huang, W. Wang, M. Bates, and X. Zhuang, "Three-dimensional super-resolution imaging by stochastic optical reconstruction microscopy," *Science*, vol. 319, no. 5864, pp. 810–813, 2008.

[25] A. Pertsinidis, Y. Zhang, and S. Chu, "Subnanometre single-molecule localization, registration and distance measurements," *Nature*, vol. 466, pp. 647–651, July 2010.

[26] M. Mlodzianoski, J. Schreiner, S. Callahan, K. Smolkova, A. Dlaskova, J. Santorova, P. Jezek, and J. Bewersdorf, "Sample drift correction in 3D fluorescence photoactivation localization microscopy," *Opt. Express*, vol. 19, no. 16, pp. 15,009–15,019, 2011.

[27] C. Geisler, T. Hotz, A. Schönle, S. W. Hell, A. Munk, and A. Egner, "Drift estimation for single marker switching based imaging schemes," *Opt. Express*, vol. 20, no. 7, pp. 7274–7289, 2012.

[28] R. Nieuwenhuizen, S. Stallinga, and B. Rieger, "Visualization and resolution in localization microscopy," in *Cell Membrane Nanodomains: From Biochemistry to Nanoscopy*. New York: Taylor & Francis, 2014, pp. 409–430.

[29] M. Juette, T. Gould, M. Lessard, M. Mlodzianoski, B. Nagpure, B. Bennett, S. Hess, and J. Bewersdorf, "Three-dimensional sub 100 nm resolution fluorescence microscopy of thick samples," *Nat. Methods*, vol. 5, no. 6, pp. 527–529, 2008.

[30] S. R. P. Pavani, M. A. Thompson, J. S. Biteen, S. J. Lord, N. Liu, R. J. Twieg, R. Piestun, and W. E. Moerner, "Three-dimensional, single-molecule fluorescence imaging beyond the diffraction limit by using a double-helix point spread function," *Proc. Natl. Acad. Sci. USA*, vol. 106, no. 9, pp. 2995–2999, 2009.

[31] M. Bates, B. Huang, G. T. Dempsey, and X. Zhuang, "Multicolor super-resolution imaging with photo-switchable fluorescent probes," *Science*, vol. 317, no. 5845, pp. 1749–1753, 2007.

[32] L. S. Churchman, Z. Okten, R. S. Rock, J. F. Dawson, and J. A. Spudich, "Single molecule high-resolution colocalization of Cy3 and Cy5 attached to macromolecules measures intramolecular distances through time," *Proc. Natl. Acad. Sci. USA*, vol. 102, no. 5, pp. 1419–1423, 2005.

[33] S. Holden, S. Uphoff, and A. Kapanidis, "Daostorm: An algorithm for high-density super-resolution microscopy," *Nat. Methods*, vol. 8, no. 4, pp. 279–280, 2011.

[34] F. Huang, S. Schwartz, J. Byars, and K. Lidke, "Simultaneous multiple-emitter fitting for single molecule super-resolution imaging," *Biomed. Opt. Express*, vol. 2, no. 5, pp. 1377–1393, 2011.

[35] E. Mukamel, H. Babcock, and X. Zhuang, "Statistical deconvolution for superresolution fluorescence microscopy," *Biophys. J.*, vol. 102, no. 10, pp. 2391–2400, 2012.

[36] L. Zhu, W. Zhang, D. Elnatan, and B. Huang, "Faster STORM using compressed sensing," *Nat. Methods*, vol. 9, no. 7, pp. 721–726, 2012.

[37] E. J. Candes and C. Fernandez-Grandam, "Towards a mathematical theory of super-resolution," *Commun. Pure Appl. Math.* vol. 67, no. 6, pp. 906–956, 2014.

[38] S. Cox, E. Rosten, J. Monypenny, T. Jovanoivc-Talisman, D. Burnette, J. Lippincott-Schwartz, G. Jones, and R. Heintzmann, "Bayesian localization microscopy reveals nanoscale podosome dynamics," *Nat. Methods*, vol. 9, no. 2, pp. 195–200, 2012.

[39] R. Nieuwenhuizen, K. Lidke, M. Bates, D. Leyton Puig, D. Grünwald, S. Stallinga, and B. Rieger, "Measuring image resolution in optical nanoscopy," *Nat. Methods*, vol. 10, no. 6, pp. 557–562, June 2013.

[40] P. Sengupta, T. Jovanovic-Talisman, D. Skoko, M. Renz, S. Veatch, and J. Lippincott-Schwartz, "Probing protein heterogeneity in the plasma membrane using PALM and pair correlation analysis," *Nat. Methods*, vol. 8, no. 11, pp. 969–975, 2011.

[41] D. Owen, C. Rentero, J. Rossy, A. Magenau, D. Williamson, M. Rodriguez, and K. Gaus, "PALM imaging and cluster analysis of protein heterogeneity at the cell surface," *J. Biophoton.*, vol. 3, no. 7, pp. 446–454, 2010.

[42] A. Löschberger, S. van de Linde, M. Dabauvalle, B. Rieger, M. Heilemann, G. Krohne, and M. Sauer, "Super-resolution imaging visualizes the eightfold symmetry of gp210 proteins around the nuclear pore complex and resolves the central channel with nanometer resolution," *J. Cell Sci.*, vol. 125, no. 3, pp. 570–575, 2012.

[43] A. Szymborska, N. Marco, A. de Daigle, V. Cordes, J. Briggs, and J. Elllenberg, "Nuclear pore scaffold structure analyzed by super-resolution microscopy and particle averaging," *Sci. Express*, vol. 341, no. 6146, pp. 655–658, Aug. 2013.

[44] S. B. van Engelenburg, G. Shtengel, P. Sengupta, K. Waki, M. Jarnik, S. D. Ablan, E. O. Freed, H. F. Hess, and J. Lippincott-Schwartz, "Distribution of ESCRT machinery at HIV assembly sites reveals virus scaffolding of ESCRT subunits," *Science*, vol. 343, no 6171, pp. 653–656, 2014.

[SP]